Article

Disorder−Order Interplay of a Barnacle Cement Protein Triggered by Interactions with Calcium and Carbonate Ions: A Molecular Dynamics Study

Akshita Kumar, Harini Mohanram, Jianguo Li, Hortense Le Ferrand, Chandra S. Verma,* and Ali Miserez*

Read Online

ACCESS | Metrics & More | Article Recommendations | SI Supporting Information

ABSTRACT: Barnacles strongly adhere to immersed solid substrates using a mixture of cement proteins (CP) that self-assembles into a permanently bonded layer and binds the barnacles' shells to foreign surfaces. MrCP20 from *Megabalanus rosa* has been identified as a putative interfacial CP; however, its functional role remains uncertain. Since the barnacle shell is primarily composed of calcite, we carry out molecular dynamics simulations to investigate the molecular interactions between MrCP20 and calcium carbonate (in free ionic form and as calcite surface). We find that MrCP20 sequesters free Ca^{2+} and CO_3^{2-} ions on its highly charged surface through disorder−order interplay of the protein and ions. A similar ordering is seen in the protein conformational landscape upon interactions with the calcite surface. Structural examinations indicate that the energetically favorable interactions with calcium carbonate are mediated by charged functional groups that flank the structured regions of MrCP20 and networks of water molecules. *In vitro* biomineralization experiments and X-ray diffraction indicate that MrCP20 favors the precipitation of the less stable vaterite polymorph of $CaCO_3$. Our study suggests that the barnacles exploit the semi-(dis)ordered nature of acidic MrCP20 to adhere to surfaces like calcite, thereby regulating nucleation, growth, or morphology of the mineral, while simultaneously interacting with other biomolecules in cement.
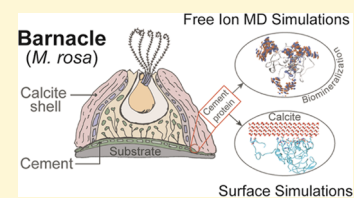
INTRODUCTION

Barnacles are crustaceans that adopt a sessile lifestyle. They permanently attach to underwater solid substrates and are capable of resisting dislodgment from strong mechanical forces. During their life cycle, barnacles transition from free-swimming nauplius and cyprids (planktonic phase) into juveniles with an adult morphology (sessile phase).[1−6] The barnacle cyprid settlement is initiated by spreading of an adsorbed layer of adhesive proteins, called the cement, to anchor itself to the foreign substratum.[7−10] Barnacle metamorphosis involves sequential morphological changes resulting in a disk-shaped basis parallel to the substratum from the juvenile stage.[11] Eventually, these shell plates calcify into an armored shell,[11,12] providing protection from predators and extreme environmental conditions in which they thrive.[13] As the barnacle grows, its calcified base and side plates continue to expand, while the animal molts through its life. The adhesive cement exudes from the cement glands and joins two different materials:[10,14] the barnacle's own calcareous base and the foreign substrata. The ability of barnacles to strongly bind to diverse substrata under an aqueous environment has prompted many studies to elucidate the biochemical and structural factors that regulate its permanent adhesion, with implications in the prevention of marine biofouling[15,16] and in the development of bioinspired adhesives that can cure in and resist aqueous environments.[17]

Although research on barnacle underwater adhesion has accelerated in the past decade,[18−25] the insoluble nature of the cement makes it difficult to dissect the specific functions of each cement protein (CP), and the molecular mechanisms involved remain obscure.[20,26,27] While many questions remain open, it has been postulated that their tenacious attachment occurs via ionic interactions and mechanical interlocking.[13] Furthermore, atomic force microscopy and surface spectroscopic characterizations of the base plate have shown that CPs also self-assemble into amyloid-like cross-β nanofibrils at the base plate/substrate interface, prompting investigators to suggest an adhesive role for these CP-based nanofibrils.[28,29] Experimental studies also support the hypothesis that barnacle interface development is a complex phenomenon coupled with sequential, timed secretory events as well as morphological changes.[12] The interface concomitantly fulfills the roles of adhering to the substratum as well as permitting radial expansion of calcified base plates and continuous molting.[12] Sequence analysis studies by Evans et al.[30] (on mollusk aragonite-associated proteins) and Pendola et al.[31] (spicule matrix proteins) indicated the presence of signature features such as intrinsically disordered regions and amyloid-like motifs.
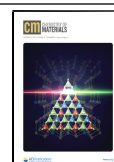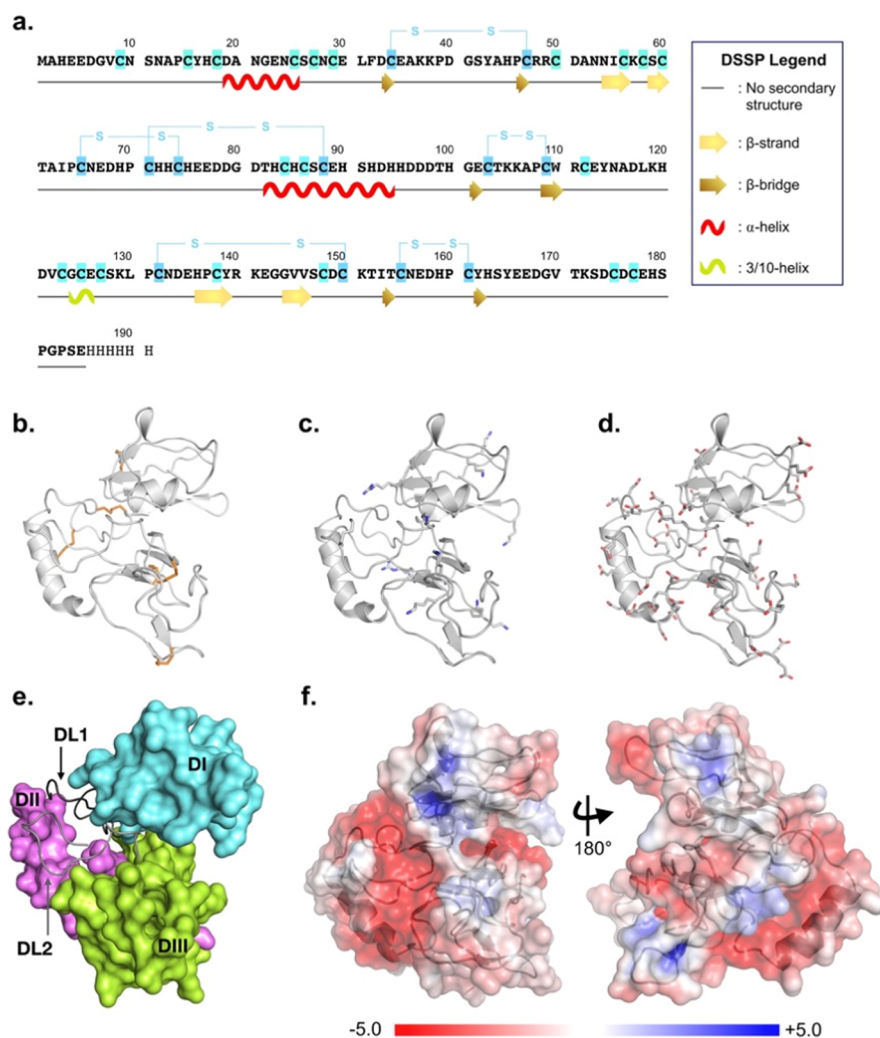
Figure 1. Structural features of MrCP20. (a) Primary and secondary structure content. (b−d) Cartoon representation of an energy-minimized NMR-derived solution structure (PDB: 6LEK) showing the spatial organization of the side chains of disulfide-bonded cysteine residues (b), cationic residues (c), and anionic residues (d) represented in sticks. (e) Multidomain tertiary conformation with three structured domains (DI, cyan; DII, magenta; and DIII, green) in surface representation, connected by two dynamic loops marked as DL1 (black) and DL2 (gray). (f) Calculated electrostatic potential on the protein surface; colors represent −5 kT/e (red) to +5 kT/e (blue).

The presence of such regions was correlated to matrix assembly as well as to mineralization.

In *Megabalanus rosa*, at least five CPs have been identified and proposed to be located in specific layers of the whole cement.[26,32−37] Among these, the 20 kDa *M. rosa* CP 20 (MrCP20) is of particular interest owing to its biochemical composition and structural characteristics.[38] It has been chemically characterized in previous studies,[14,38−40] and we recently reported the tertiary structure of recombinant full-length MrCP20 using solution-state nuclear magnetic resonance (NMR) spectroscopy and molecular dynamics (MD) simulations.[41] In this study, we investigated the influence of the small number of hydrophobic residues together with the high percentage of charged residues (Arg 2%, Lys 5%, Asp 11%, and Glu 10%) on the dynamic nature of the protein, which enables its adaptation into multiple conformations. The identified conformations exhibit partial disorder along with some secondary structural motifs that are conserved during the MD simulations (and likely have functional implications). Based on the sequence composition of MrCP20 and its ability to adopt multiple meta-stable conformations,[41] it is hypothe-

sized to play essential roles in the multifunctional process of underwater attachment,[9,14] specifically in regulating the growth of the biomineralized shell and joining the calcareous base with cement.[42]

Mori et al. demonstrated that MrCP20 preferentially adheres to calcite over other minerals found in the marine environment.[14] Kamino et al. suggested that MrCP20 (along with MrCP19[23]) plays a key surface-coupling role. Based on the principle that protein function is closely related to its location, it was also postulated that MrCP20 is located at the interface between the calcite base and bulk cement.[37,42] The selective adhesion of MrCP20 suggests noncovalent interactions with the calcite base plate since the latter lacks any reactive functional groups.[42] Sequence and structural analyses of MrCP20 indicate the presence of clusters of charged amino acids, which may facilitate the protein in coordinating inorganic ions.[38,41] The inability of MrCP20 to adsorb onto other positively charged polymers[14] further suggests that electrostatic interactions and the spatial arrangement of MrCP20's surface residues may play critical roles during adsorption and calcite adhesion. So et al. revealed that

MrCP20 has the ability to selectively interact with atoms on the $\{10\bar{1}4\}$ face of the calcite[19] surface and subsequently assembles into nanofibrils. Their work also highlighted that cooperative protein interactions play a role in shaping the growing crystal.[19] Other reports point that MrCP20 homologues found in transcriptome datasets of other barnacles (*Augochlora amphitrite* and *Fistulobalanus albicostatus*) are also rich in charged amino acids and are predominantly present in the calcareous base plate.[43] In contrast, a transcriptomic study of *Tetraclita japonica formosana*[44] (which does not have a calcareous plate) highlighted the absence of MrCP20 homologues.

Taken together, these studies suggest the possibility of MrCP20 playing an active role in calcite base coupling. Calcite is a major constituent of the barnacle shell and, given that barnacles are known to be a gregarious species, often living in dense clusters, calcite is likely a common substrate for cement attachment. However, details of the molecular mechanisms of interactions between CP and calcite in barnacles remain poorly understood. To explore the underlying mechanisms, we hypothesize the following possible functionalities associated with putative interfacial MrCP20: (i) it self-assembles into an ordered substrate for heterogeneous or homogeneous mineralization of calcite; and/or (ii) it sequesters the Ca^{2+} and CO_3^{2-} ions (or their complexes) for crystallization; and/or (iii) it ultimately interacts with the homogeneous calcite surface. Previous studies have suggested the importance of intrinsically disordered proteins (IDPs) and peptides in biomineralization.[45–47] However, mechanistic details at the molecular level as well as the thermodynamics of binding to such surfaces remain unclear.[45] MD simulations are increasingly being employed to elucidate complex protein-biomineral systems,[48–52] and we use them here to explore the hypothesized functions of MrCP20. The recent experimental determination of the structure of MrCP20 by solution NMR[41] gives us the opportunity to explore the significance of charged surface residues (Figure 1) in the context of adhesive molecular mechanisms and the likely functional roles of MrCP20 as one of the constituents of the proteinaceous cement.

Based on the aforementioned experimental observations,[14,19,44] we examined the association of MrCP20 with free Ca^{2+} and CO_3^{2-} ions as well as its adsorption onto the $\{10\bar{1}4\}$ face of calcite using all-atom MD simulations. We develop models suggesting how acidic MrCP20 regulates free Ca^{2+}- and CO_3^{2-}-ion assembly around the protein, in close agreement with experimental observations. We determine the role of charged residues along with hydrogen-bond donors and acceptors in sequestration of free ions and how further stabilization of the assembly is achieved with water-mediated interactions. Additionally, we find that ion assembly around the protein is coupled to structural ordering of the protein. The simulations of MrCP20 bound to the calcite surface suggest that the conformational flexibility of the protein promotes efficient mediation of adhesion with the ordered calcite surface, both directly through electrostatic interactions and indirectly through water-mediated interactions.

■ METHODS

Molecular Dynamics (MD) Simulations: MrCP20 in the Presence of Ca^{2+} and CO_3^{2-}. Model-1 from the NMR ensemble of MrCP20[41] represents the lowest energy conformation and hence was chosen as the initial coordinates for our modeling studies. The side-

chain conformations of Asn and His residues were optimized, protonation states of ionizable residues were assigned, and missing hydrogen atoms were added using PDB 2PQR.[53] We investigated the structural dynamics of a mixture of MrCP20, water, and Ca^{2+} and CO_3^{2-} ions, varying the concentrations of the latter to be 0.12, 0.67, and 1.49 M. A single molecule of MrCP20 was centered in a box of dimensions 79.1 Å × 79.1 Å × 79.1 Å and the concentrations of Ca^{2+} and CO_3^{2-} and the number of water molecules were varied, with each box corresponding to one of the three ionic concentrations. The ratio of Ca^{2+} and CO_3^{2-} to water molecules mimics the unsaturated to saturated ionic conditions, and was calculated to systematically simulate the ambient conditions (details in Supporting Information Methods). The initial configurations of the ions were generated by randomly placing the required number of Ca^{2+} and CO_3^{2-} ions using the program PACKMOL[54] (with the minimum distance between the ions set to 2.2 Å). The net charge on each box was neutralized with appropriate numbers of Na^+ counterions, and finally, the molecules were solvated with TIP3P[55] water molecules. The details of each simulation are given in Table 1. The parameters for CO_3^{2-} were

Table 1. System Details for the MD Simulations

system name	macroscopic ion concentration (M)[a]	Ca^{2+} and CO_3^{2-} pairs	total water molecules	simulation time (ns)
CC$_{low}$	0.12	30	13 804	3 × 100
CC$_{medium}$	0.67	149	12 379	3 × 100
CC$_{high}$	1.49	298	11 116	3 × 100

[a]Concentration based on ion/water ratio.

generated using *Antechamber*,[56] and the protein and Ca^{2+} ions were modeled using the all-atom version of Amber 99SB force-field (ff99SB)[57] and the GAFF[58] force field, respectively.

Energy minimization and MD simulations were performed with the Sander and PMEMD modules of AMBER14.[59] All bonds involving hydrogen atoms were constrained using the SHAKE[60] algorithm, enabling a time step of 2 fs during the MD simulations. Periodic boundary conditions were used, and a distance cutoff of 9 Å was selected to calculate the nonbonded interaction energies. The long-range electrostatic interactions were evaluated using the particle mesh Ewald (PME) method.[61] The initial optimization of the structures was carried out by imposing positional restraints on the protein atoms followed by 250 cycles of steepest descent and 250 cycles of conjugate gradient energy minimizations. This was followed by MD simulations on the system in a stepwise manner including nine equilibration simulations of 100 ps each, during which the system was first heated gradually to 300 K at constant volume and then equilibrated at a constant pressure of 1 atm. Subsequently, unrestrained equilibration (1 ns) and production runs were performed at a constant temperature (300 K) using a Berendsen temperature coupling scheme and constant pressure (1 atm) using the Berendsen barostat.[62] The final production simulations were carried out for 100 ns (in triplicate). Analysis of the sampled conformations was carried out by computing their root-mean-square deviations (RMSD) against the starting structure, average atomic fluctuations, and ion occupancy grids (binning atoms into 1 Å × 1 Å × 1 Å grid cells), using the *ptraj* module in AMBER. Simulation trajectories were visualized using VMD.[63] Figures were generated using VMD or PyMOL,[64] and occupancy maps were generated using Chimera.[65] Plots were generated using the Graphing, Advanced Computation and Exploration (GRACE) program.[66]

Molecular Dynamics (MD) Simulations: MrCP20 in the Presence of Calcite Surface. A model of a calcite slab with a $\{10\bar{1}4\}$ face was constructed using the Materials Studio[67] software for simulating the adsorption of MrCP20 on this face; it has been observed that MrCP20 interacts with the $\{10\bar{1}4\}$ face of the calcite surface.[19] We constructed a four-layer calcite slab, approximately (7 nm × 7 nm) in the xy direction and 1.2 nm in the z direction. The MrCP20 protein structure prepared for the ionic simulations above was also used for these simulations. Since the slab is only four layers

thick, we carried out an extra simulation using a 12-layered calcite slab (details in the Supporting Information). The slab geometry was found to be stable in the simulations of both the four-layered and 12-layered slabs (Supporting Information Figure S1). Hence, we focus on the four-layered calcite slab in this study as the smaller size enabled us to carry out detailed simulations exploring the interfacial adsorption properties of MrCP20.

The MD simulations were performed using the GROMACS suite (5.0.4)[68] of programs employing the AMBER force-field set (ff99SB)[57] for consistency with the other simulations in this study. Parameters for calcite, calcite–water, and calcite–protein interactions were modeled based on published work.[69,70] Given the lack of experimental data on a starting state, we generated four starting states. Each state was defined by the MrCP20 in a unique orientation, located at ∼5 nm (distance between the centers of mass of the protein and of calcite) from the $\{10\bar{1}4\}$ face of calcite. Each system was solvated with TIP3P[55] water molecules and Na$^+$ counterions were incorporated to neutralize the net charge on each system. Each system was first subjected to energy minimization using the steepest descent algorithm for 500 steps, followed by 100 ps of position restrained on protein and calcite surface MD simulations. Subsequently, each system was subjected to an unrestrained equilibration run for 1 ns and 500 ns of the production simulations. During the simulations, periodic boundary conditions were used; short-range electrostatic interactions and van der Waals interactions were calculated using a cutoff value of 0.9 nm, whereas the long-range electrostatic interactions were calculated using particle mesh Ewald summation.[61] The simulations were performed in the NPT ensemble, with semi-isotropic coupling. The temperature and pressure were maintained at 300 K and 1 bar, respectively (using Nose–Hoover[71] thermostat and Parrinello–Rahman[72,73] barostat coupling scheme, respectively). Trajectory analysis was done with built-in functions in GROMACS 5.0.4. VMD[63] was used for visualization of trajectories, analysis, and illustrations. Plots were generated using the program GRACE.[66]

Mineralization by Vapor Diffusion. Slow-growth mineralization experiments were set up on submerged glass coverslips following the well-established techniques of using ammonium carbonate vapor diffusion through calcium carbonate solution.[19,74,75] The coverslips were cleaned and rinsed with deionized water and placed in a Nunc 24-well plate, each submerged in 7.5 mM CaCl$_2$ solution. MrCP20 was expressed and purified following the protocol mentioned in Mohanram et al.[41] For mineralization experiments, the purified protein in Tris-buffered saline was dialyzed (Spectra/Pro Dialysis membrane, MWCO: 3000 Da) twice against 7.5 mM CaCl$_2$ for 3 h at room temperature. The pH was adjusted to 7.5 by the addition of 0.67 M NaOH, and the protein was introduced into the wells in the Nunc 24-well plate. The concentration of the final protein solution was adjusted to 0.001 and 0.005 mg/mL. The plates were wrapped with aluminum foil, punctured with two pinholes, and placed in a small desiccator that additionally contained a beaker of ammonium carbonate. Typically, the mineralization reaction was allowed to stand for 7 days. The morphology of the crystals was characterized using scanning electron microscopy (SEM).

Scanning Electron Microscopy (SEM). The calcium carbonate crystals were characterized using field emission SEM (JOEL 7600F) at an accelerating voltage of 10 kV. The coverslips were secured onto the SEM mounts using carbon tape ensuring a conductive pathway for imaging. The mounts were coated with platinum and imaged at a working distance of 12.00 mm.

Powder X-ray Diffraction (XRD). The composition of the dried crystals in the presence and absence of MrCP20 was verified using powder XRD (Empyrean, Malvern PANalytical). Using Cu Kα radiation and by scanning the sample through a range of 2θ angles (15−65°, scanning rate of 0.03°/s), the lattice diffraction peaks were acquired. The diffraction peaks were assigned using the 2θ range from the American Mineralogist Crystal Structure Database[76] (AMCSD) codes 0004854 and 0000098 for vaterite and calcite, respectively.

■ RESULTS AND DISCUSSION

Ionic Structure around MrCP20. Nucleation, growth, or inhibition of mineral phase in biomineralized structures requires protein–mineral interactions.[77,78] In general, acidic moieties in biomolecules are known to be involved in regulating mineralization.[45,46,79−84] Assuming that the acidic MrCP20 (Figure 1) in the cyprid adhesive plaque interacts with the shell plates during calcification,[11] we hypothesize that it might be involved in unidirectional regulation (or inhibition) of mineralization, thus enabling the cement adhesive to develop. This leaves a fundamental question: what are the potential interaction sites in MrCP20 that may associate with Ca^{2+} and CO$_3^{2-}$ ions? We tested the effects of three ionic concentrations (0.12, 0.67, and 1.49 M, named as **CC$_{low}$**, **CC$_{medium}$**, and **CC$_{high}$** respectively; Table 1) to probe the influence of a mixture of Ca^{2+} and CO$_3^{2-}$ ions on the dynamics of MrCP20 and to explore the interactions between the protein and calcite through MD simulations. As a control, we also carried out a simulation of only the ions in explicit solvent and compared it with simulations of the protein[41] in solvent without ions. Each simulation was carried out for 100 ns in triplicate (total sampling time of 300 ns for each system) with different initial ionic (Ca^{2+} and CO$_3^{2-}$) distributions.

At the beginning of the simulations, the ions are distributed randomly around the protein (or in the protein-free control simulations). In the control system, we observe that the ions cluster into one dense mass (Figure 2a). However, in the
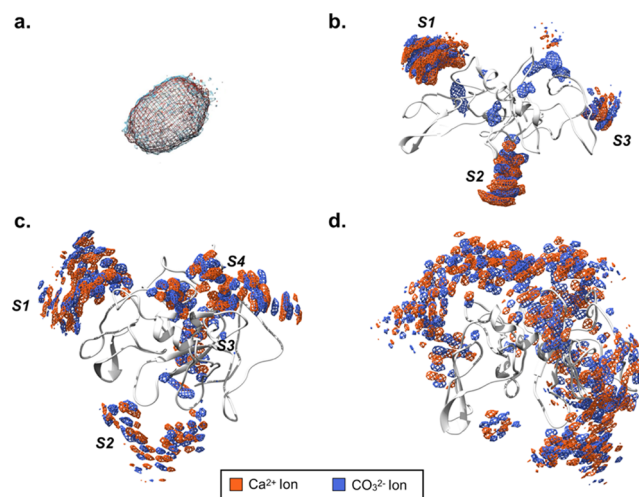

Figure 2. Ion density maps around MrCP20. Ca^{2+} and CO$_3^{2-}$ ions are represented in orange and blue meshes, respectively. (a) Ion (0.12 M concentration) cluster in the absence of MrCP20. (b−d) Ion clusters in the presence of MrCP20 around the protein surface for ionic concentrations of 0.12 M/CC$_{low}$ (b), 0.67 M/CC$_{medium}$ (c), and 1.49 M/CC$_{high}$ (d).

presence of MrCP20, the ions disperse around the protein surface, leading to the appearance of multiple cluster sites (Figure 2b−d). To evaluate the differences among various ionic systems, we examined the root-mean-square deviation (RMSD) of the protein as the simulations progressed. The deviations are similar in the first 30−50 ns and then appear to diverge somewhat (2−3 Å) (Supporting Information Figure S2a). Relatively lower RMSD values are seen when the ionic concentrations are high, which arise from the structural order/stability induced by the clustering of the ions around MrCP20. A similar pattern is observed for the root-mean-square
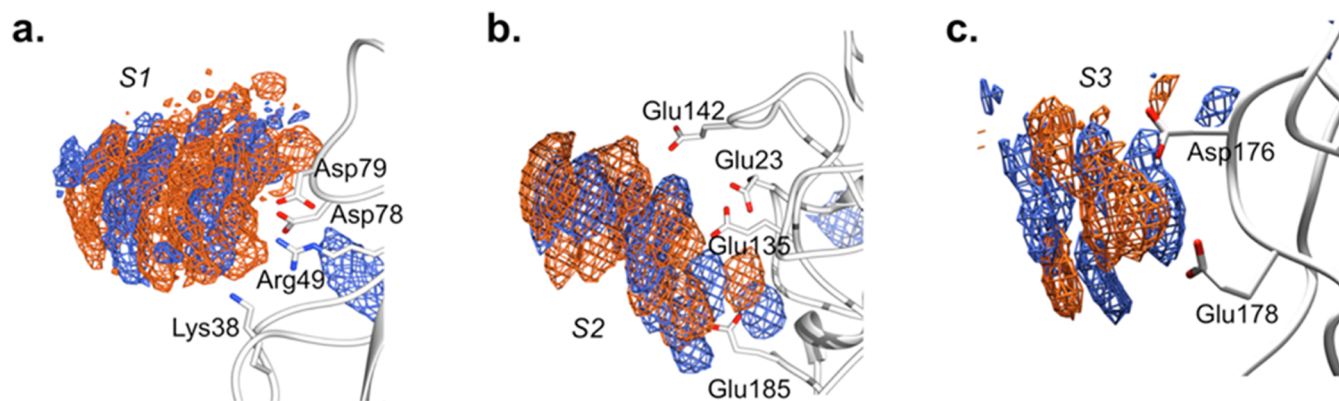
Figure 3. Ion density maps for CC_{low} (0.12 M Ca^{2+} and CO_3^{2-} ions). MrCP20 is represented in white cartoon. The occupancy maps for calcium are shown in orange mesh, and carbonate in blue mesh. Three cluster sites are identified, where the ions probe interactions with the surface of MrCP20 during the MD simulations. Residues engaged in interactions at (a) site 1 (S1), (b) site 2 (S2), and (c) site 3 (S3) are highlighted in white sticks.

fluctuations (RMSF); indeed, in control simulation, it is clear that in the absence of ions (i.e., protein only in explicit solvent), the protein undergoes the most fluctuations (Supporting Information Figure S2b). In summary, an ionic atmosphere thus promotes or enhances stabilization of the protein (Supporting Information Figure S2b−f). As the ionic concentration increases, the ordered regions as seen in the NMR structure undergo further stabilization together with disorder-to-order transitions in the flanking regions, thus bringing greater stability to the protein overall (Supporting Information Figure S2c−f). The dense ionic clusters are preferentially found in the vicinity of the side chains of charged residues (Arg, Lys, Glu, and Asp; Figures 3 and 4); the clusters grow until about 50 ns, after which they remain stable (Figure 2). In CC_{low}, three clusters are observed (Figure 2b). At site S1, we note the involvement of both anionic and cationic residues interacting with ions (Asp78, Asp79, Lys38, Arg49; Figure 3a), in contrast to the anionic sites S2 (Glu23, Glu135, Glu142, and Glu185; Figure 3b) and S3 (Asp176, Glu178; Figure 3c). It is clear that as the number of ions increase (0.12 to 0.67 to 1.49 M), new clusters appear around the protein surface (Figure 2). Consequently, there is an increase in the number of interacting residues at each engagement site (Figure 4 and Table S1). It is interesting that while at lower concentrations the ions protrude away from the protein surface in columnar assemblies, at the highest concentration, they disperse and envelop the protein, clearly driven by entropy (Figure 2).

Although the charged residues preferentially mediate interactions with the ions (20%, 45%, and 55% of the charged residues involved in interactions as seen in CC_{low}, CC_{medium}, and CC_{high} respectively), polar groups such as Ser, Thr, Asn, and Tyr also mediate some interactions (Table S1). Among the charged residues, anionic residues predominate in engaging interactions (likely as a consequence of the protein surface being negatively charged). Experimental observations on single anionic residues (Asp and Glu) have shown that these amino acids stabilize Ca^{2+} and CO_3^{2-} clusters in solution.[85] Assemblies of Ca^{2+} and CO_3^{2-} stabilized through ionic interactions (with Asp and Glu) are relatively insoluble and develop into disordered mineral phases.[85] While acidic residues are often found in proteins involved in regulating mineralization, the cationic residues are sparingly found in such proteins.[50] In our simulations, we observe that the

cationic residues also engage in interactions with the ions (with more than 50% of the basic residues observed in mediating interactions; Figure 4 and Table S1).

The sequestration of the ions around the protein is mediated by the following interactions: (a) the CO_3^{2-} ions interact with the amine (Lys) or guanidinium (Arg) groups; (b) the ions interact with the carboxyl side-chain oxygens of the acidic residues (Asp and Glu); (c) the carboxylate groups of the acidic residues make salt-mediated and/or water-mediated interactions with the similarly charged CO_3^{2-} ions; (d) a small fraction of interactions (hydrogen bond/ionic) are also formed between the backbone nitrogen and side-chain oxygen atoms of Ser and Ca^{2+} or with the carbonate oxygen of the CO_3^{2-} ion; (e) the side-chain hydroxyl of Tyr/Thr forms electrostatic interactions with Ca^{2+} ions; and finally (f), the polar side chain of Asn coordinates both Ca^{2+} and CO_3^{2-} ions (Figures 3, 4, and 5a−c). All of the above interactions exhibit lifetimes greater than 95% of the simulations, with bond distances in the range of 1.6−2.8 Å. In addition, variations in the sign and magnitude of the charges on the protein surface dictate the stepwise organization of ions around the protein. For instance, at site S1 (in CC_{low} system), the radial density plot (of interacting residues and ions; Figure 5d) shows a subpeak at 3.1 Å, indicating the presence of carbonate in the first layer, followed by organization of calcium and carbonate ions. However, at sites S2 and S3, which are predominately anionic, inverse arrangements are observed (Figure 5e−f). Supporting these results, recent computational studies reported a preference of acidic amino acids for hydrated amorphous calcium carbonate ($CaCO_3$), explaining their involvement in the inhibition of precipitation and stabilization of a liquid phase.[50,86] Further support for our findings comes from the work of Finney et al.[86] who compared the effects of amino acids and their oligopeptides (polymer additives: Arg, Asp, and Gly) on $CaCO_3$ and concluded that (i) the number of solute-binding sites and their accessibility (which requires a certain level of conformational flexibility) to the ionic network plays a crucial role in stabilizing the dense liquid $CaCO_3$ phase and (ii) the charge distribution of the solutes may control the topology of the $CaCO_3$ network, which may lead to the inhibition or formation of the mineral.

The majority of the residues interacting with Ca^{2+} and CO_3^{2-} ions occupy the loops/turns in the MrCP20 structure. These regions are generally in the vicinity of structured motifs
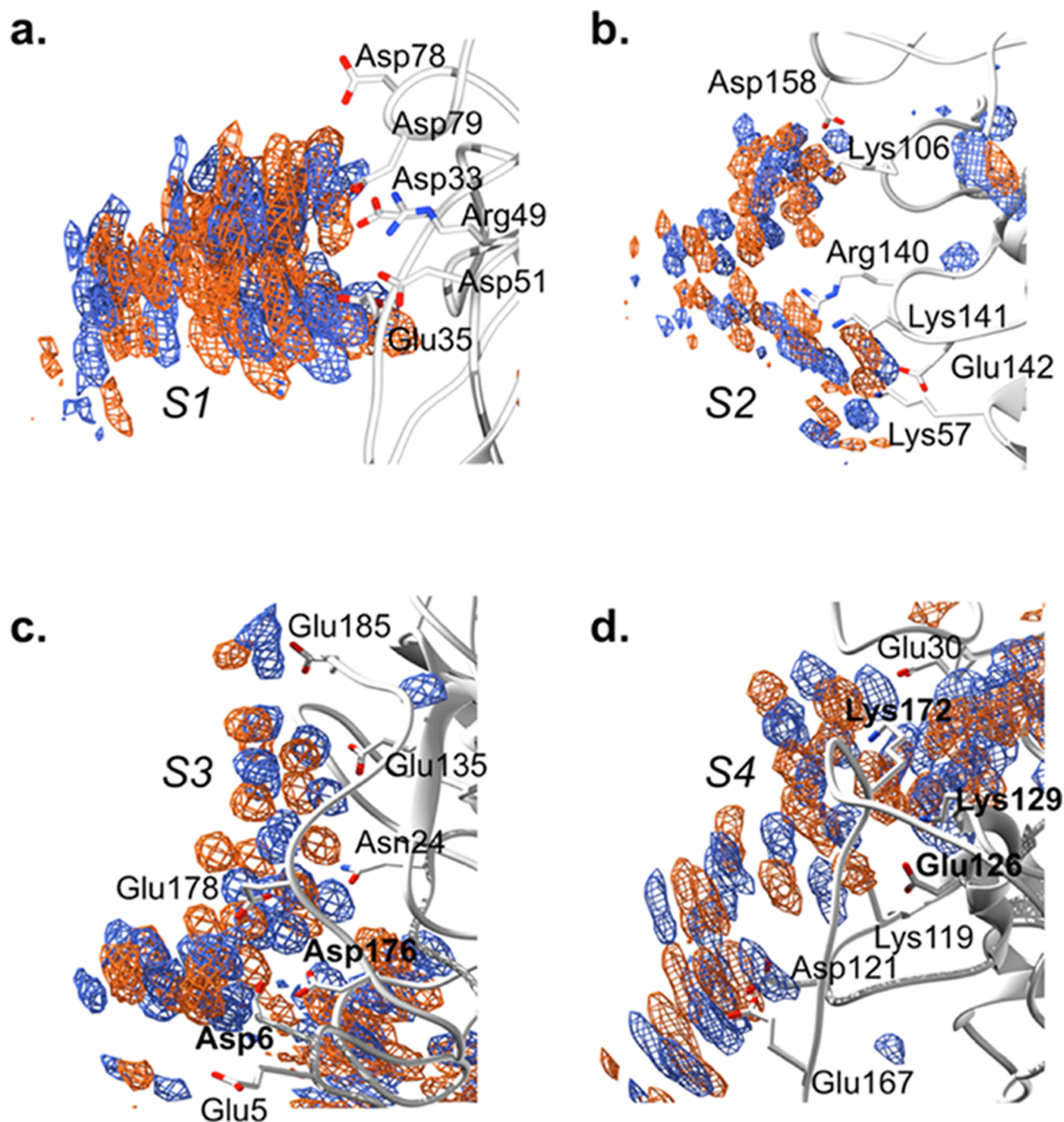
Figure 4. Ion density maps for CC_{medium} (0.67 M Ca^{2+} and CO_3^{2-} ions). MrCP20 is represented in white cartoon. The occupancy maps for calcium are shown in orange mesh, and carbonate in blue mesh. Three cluster sites are identified, where the ions probe interactions with the surface of MrCP20 during the MD simulations. Residues engaged in interactions at (a) site 1 (S1), (b) site 2 (S2), (c) site 3 (S3), and (d) site 4 (S4) are highlighted in white sticks.

or disulfide bridges (Figure 1a). It appears that their spatial proximity to the structured motifs constrains them on the surface in a manner that enhances their interactions with the ions. It is plausible that the disulfide bridges and the intrachain contacts (including those dispersed in extended β-strand regions) impart limited flexibility to the interacting regions (disordered loops and turns) and reduce labile motion, thus promoting favorable interactions between the surface residues and the ions. Further, the interactions between the ions and

MrCP20 alter the dynamics of the protein chain (Supporting Information Figure S2). In summary, the ions elicit changes in the local structure, from a semiordered, flexible configuration to a more ordered conformation, as they assemble around the protein surface. The ions provide extra stabilization to MrCP20, probably compensating for the lack of overall internal stabilization, as also observed in other systems.[84,87−89] Overall, the ionic simulations of MrCP20 in the presence of Ca^{2+} and CO_3^{2-} ions provide a refined understanding on the
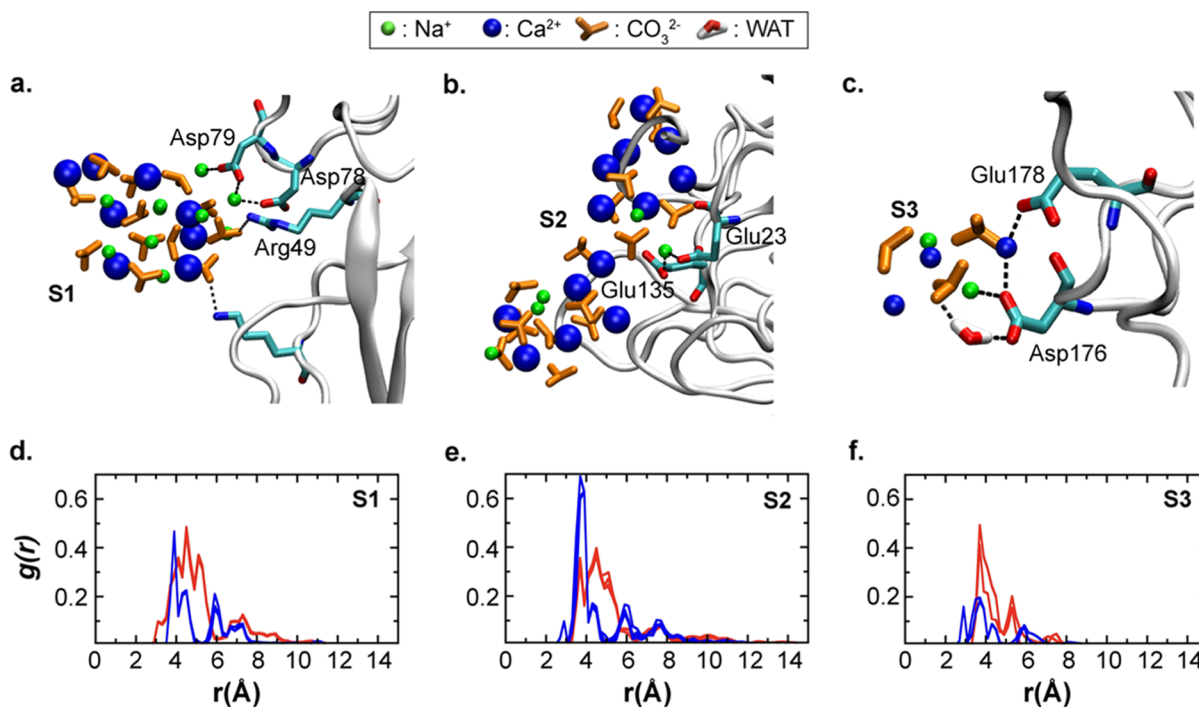
Figure 5. Ion−residue interactions in CC_{low} at sites (a) S1, (b) S2, and (c) S3. MrCP20 is shown as a white cartoon. Interacting residues are shown in cyan sticks. The dashed lines represent the interaction. (Not all interacting residues are shown for clarity and to minimize overlap). (d−f) Intermolecular radial density function between interacting residues at sites S1 (d), S2 (e), and S3 (f) with Ca^{2+} (blue) and CO_3^{2-} (red) ions.

role of key charged residues (Asp, Glu, Arg, and Lys) that facilitate ion association. It is plausible that during the natural mineralization process, the interactions between these anchoring residues and ions play a crucial role in regulating ion aggregation or in holding the new forming cement with the growing shell.

Protein Binding: MrCP20 on Calcite Surface. In the above section, we discussed how the presence of the protein attenuates the diffusion of the ions and sequesters them onto the surface of MrCP20. Given that, there are two possible scenarios for the role of MrCP20: (i) there is a preformed calcium carbonate mineral, and as it approaches the edge of the cement, the interactions with MrCP20 inhibit further growth; (ii) the mineral begins from the layer of the ions around the protein surface, and an array of proteins probably lines up to nucleate the formation of the crystal, which will grow away from the protein (or cement) surface. It is interesting that the two patterns seen, the columnar aggregation of ions at low concentrations and the diffused aggregation at high ion concentrations, can both act as nucleating centers for the rapid growth of the mineral. However, at the end of this process, MrCP20 will remain adhered to the crystal face, and this is the interaction we study next (since the process of growth of the crystal is beyond the scope of this study).

Due to a lack of experimental data on the orientation of the protein with respect to the mineral, we orient MrCP20 in four different conformations, guided by the regions of interactions with CaCO₃ seen in our simulations above. The protein was placed at 5 nm (in the z direction) from the surface and allowed to diffuse in response to the presence of calcite surface. In all of the simulations, the protein rapidly (within 200 ns) reaches the surface and engages in stable interactions for the remainder of the simulation (300 ns), at 0.2−0.3 nm from the surface (Figures 6a and 7a). At this distance, interactions

between the acidic protein and the calcite surface drive the stable association (Figure 6). The protein undergoes expansion as it reaches the surface (Figures S3a,b and 6b−e; increase in the protein's radius of gyration; Figure 7b) as the strong electrostatic interactions between the charged residues (largely anionic residues) and the ionic surface are maximized (Table 2). This ability to maximize interactions by rapid conformational adaptations underscores the highly flexible/disordered character of such acidic proteins to interact with calcite and similar inorganic surfaces (such as hydroxyapatite (HA); Supporting Information Figures S4−S6 and Tables S2 and S3; simulations with HA surface discussed in the Supporting Information).

In general, although there is a preponderance of anion-driven interactions with the calcite (Table 2), cationic and polar residues also engage in interactions with calcite. This distribution parallels the interactions seen in the MrCP20-free-ion simulations (Table S1). Once again, we note that the binding is predominantly mediated via Coulombic interactions between the acidic residues (Asp and Glu; Tables 2 and 3, and Figure 7c) and the calcium cations. The cationic amine group on the side chain of Lys residues extends to interact with CO_3^{2-} groups on the surface. We also observe polar side-chain interactions of Ser, Thr, Asn, and Tyr residues. Ser interacts with Ca^{2+} through its side-chain hydroxyl oxygen and occasionally through H-bonds between the hydroxyl hydrogen and an oxygen atom of the carbonate group. Asn interacts with Ca^{2+} ions or the oxygen of the carbonate through its side-chain carboxamide group, which can function as a hydrogen-bond donor and acceptor. Thr and Tyr facilitate binding through their polar side chains, forming H-bonds with CO_3^{2-} oxygen atom on the surface. It is interesting to note that Ser and Asn residues are also common constituents of biomineralization proteins.[79]
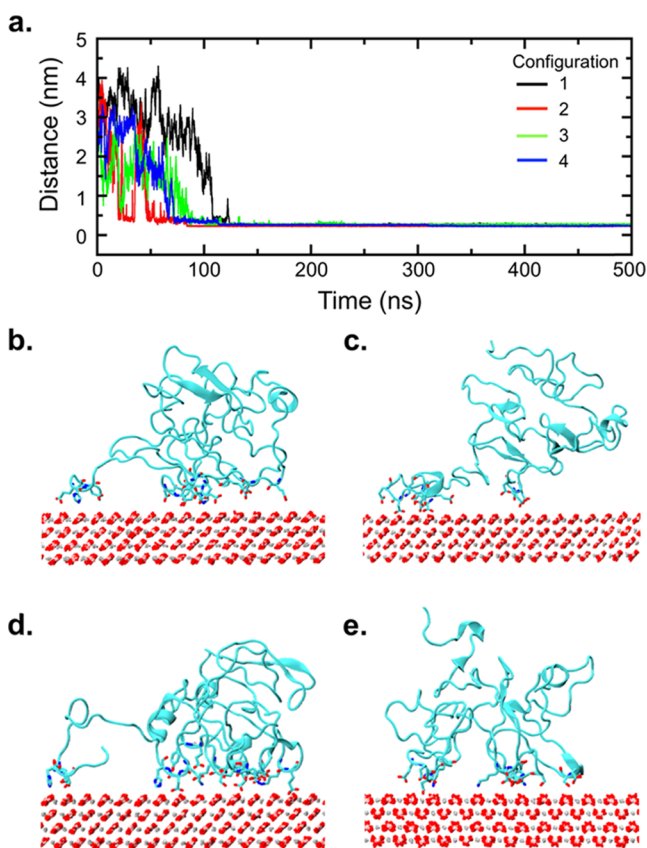
Figure 6. MrCP20 adsorption onto the $\{10\bar{1}4\}$ face of a calcite surface. (a) Distance between MrCP20 and the calcite surface over 500 ns of the MD trajectory for four different initial orientations of the protein relative to the calcite surface. (b−e) Final states of the four systems (configurations 1−4, respectively). MrCP20 is displayed as cartoons. The interacting protein residues (cyan) and calcite surface are in stick representation.

MrCP20 sequence also has a significant percentage of ionizable polar His (10.3%) that can engage in interactions

Table 2. List of MrCP20 Residues That Interact with the $\{10\bar{1}4\}$ Face of the Calcite Surface

configuration	interacting residues[a]
1	His3, Glu5, Asp6, Tyr16[b], Glu30, Asp33, Glu77, Asp81, Thr82[b], His85[b], Asp121, Glu178, Ser180, Glu185
2	Asp93, Asp96, Asp98[b], Glu166, Glu167, Asp168, Lys172, Asp174, Asp176, Glu178, Glu185
3	Glu4, Glu5, Asp6, Glu23, Asn24, Ser26[b], Lys106, Glu113[b], Tyr114, Asn133, Asp134[b], Glu135, Lys141, Glu142, Glu157, Asp158, His159[b], Asp176, Glu178, His179[b], Ser180
4	Asp40, Ser42[b], Asp51, Asn53[b], Ser59[b], Thr61[b], Glu76[b], Glu77, Asp78, Asp79, Lys119, Lys141, Glu142

[a]Residue sequence number taken from ref 41. [b]Not identified as an interacting residue in ionic simulations.

with the CO_3^{2-} oxygens. In simulations, we observe that His residues, spatially organized near the interacting acidic residues, participate in calcite binding. It is probable that these His residues in the highly acidic local environment exhibit dynamic changes in charge and protonation states to facilitate interactions with the oxygen atoms of CO_3^{2-} on the surface.[74,79] An experimental study of a Cys-, His-, and Arg-rich protein (called Perlinhibin) from the nacreous layer of a sea snail indicated that this protein specifically interacted with the calcite steps, inhibiting further crystal growth at the interaction sites,[74] in corroboration with our hypothesis and simulations.

Overall, while the protein is conformationally labile, the disulfide bridges do constrain the conformational landscape that the protein can occupy. Most of the secondary structure motifs identified by NMR remain conserved during the course of simulations (Figure S3c). The residues that interact with the mineral surface are distant from the disulfide bridges and are spatially distributed (or organized) in the turns or disordered regions, and therefore highly flexible. This flexibility aids the conformational lability associated with rapid restructuring that accompanies maximizing interactions. Energetic analysis reveals that electrostatic interactions are the key drivers of the association between the protein and the calcite surface,
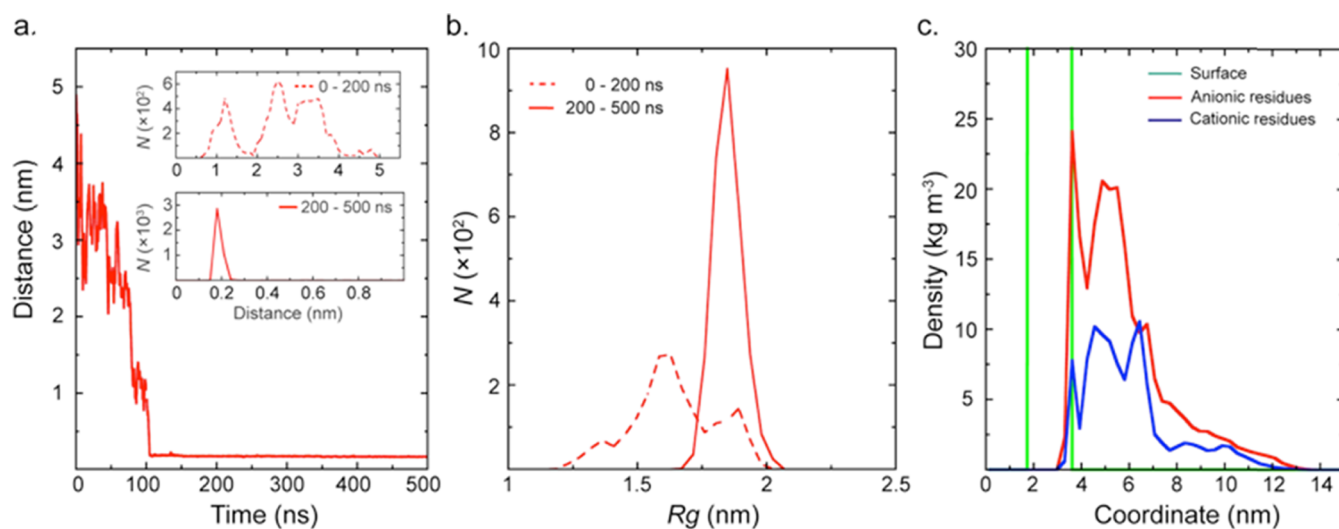

Figure 7. Interactions of MrCP20 with the $\{10\bar{1}4\}$ calcite surface. (a) Distance between MrCP20 and the surface over 500 ns. The insets show the probability distance distributions between (top) 0−200 ns and (bottom) 200−500 ns. (b) Probability distribution of the radius of gyration of MrCP20: 0−200 ns (dotted red line) and 200−500 ns (full red line). (c) Density of anionic (red) and cationic (blue) residues around the calcite surface (green).

Table 3. Number of Water-Mediated Interactions between the Protein and the Calcite Surface (N_{pwc}), Number of Water Molecules Released from the Calcite Surface upon Protein Adsorption (N_{wr}), and Protein Adsorption Energies for the Respective Configurations

configuration	N_{pwc}	N_{wr}[a]	total energy (kJ/mol)[b]	Coulombic energy (kJ/mol)[b]	energy ASP + GLU (kJ/mol)[b]
1	2.9 ± 1.7	10.3 ± 1.2	−148.4 ± 5.9	−77.2 ± 2.2	−54.6 ± 8.9
2	5.2 ± 1.9	11.2 ± 1.8	−241.5 ± 8.2	−170.4 ± 3.9	−79.5 ± 14.1
3	8.7 ± 2.1	21.6 ± 3.1	−480.3 ± 12.9	−386.3 ± 9.0	−180.4 ± 9.6
4	6.1 ± 1.5	17.4 ± 2.6	−324.1 ± 12.1	−237.3 ± 10.1	−118.0 ± 12.5

[a]Difference calculated by computing the number of calcite surface-bound water molecules in the first 50 ns (protein not bound to calcite surface) and last 50 ns (protein bound to calcite surface) of the MD trajectory. [b]The configurational energy component.
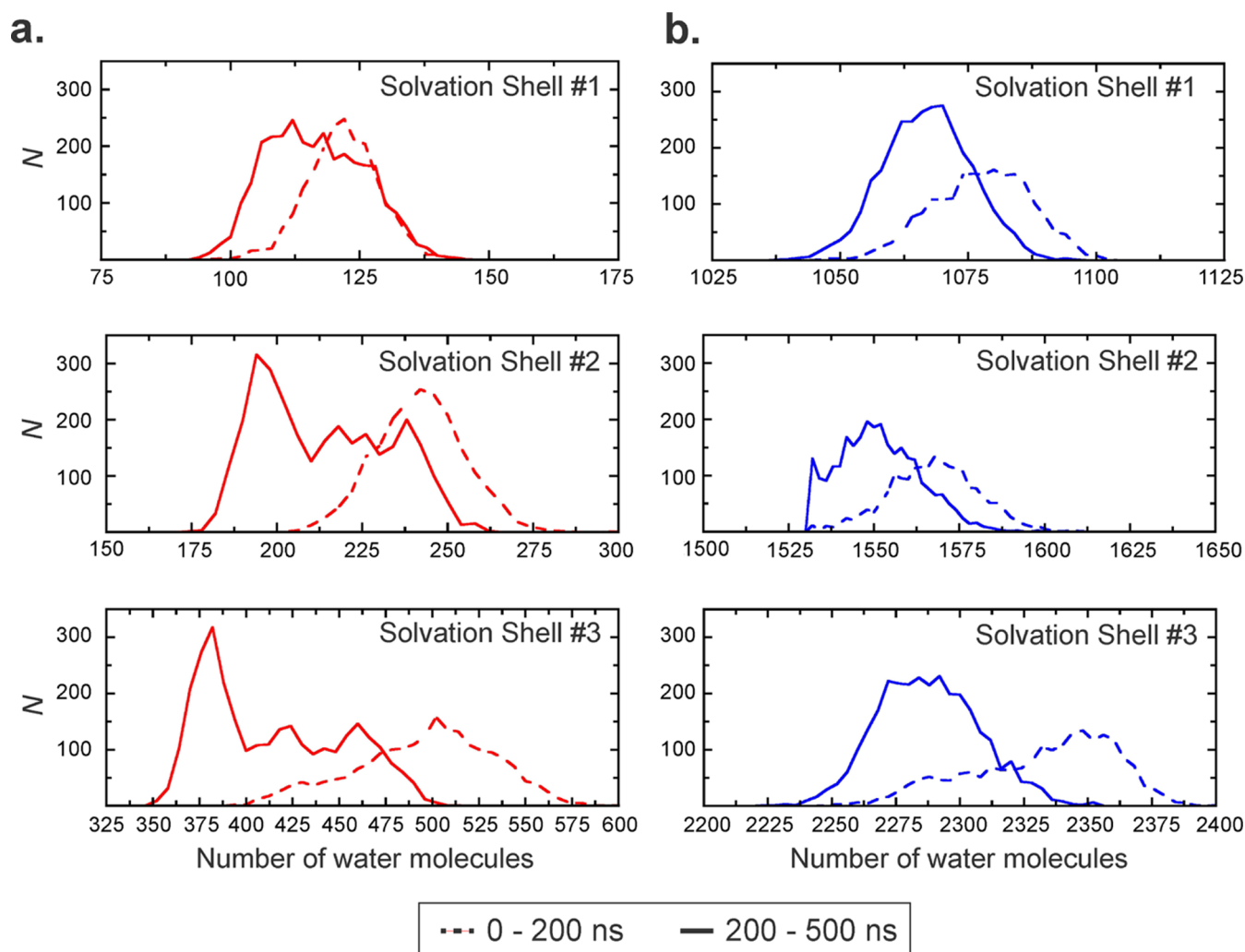

Figure 8. Number of water molecules around (a) the interacting residues in MrCP20 (red) and (b) the calcite surface (blue) in the first (0.35 nm), second (0.5 nm), and third (0.7 nm) coordination shells for the initial 200 ns (dotted lines) and the final 300 ns (full line).

with most interactions emerging from the negatively charged residues (Asp/Glu) (Tables 2 and 3). Variation in energies reflects the likelihood that multiple regions of the protein can interact with the surface, without preference for any single motif. For example, in configuration 3, residues from various regions of MrCP20 extensively interact with the surface (Figure 6), while relatively limited localized interactions are detected in other configurations (Table 2). Electrostatic interactions between the protein and the model surface, calcite, dominate. We explore this further by carrying out two additional simulations, one with a model oxide surface (regular silica slab; Supporting Information Figure S7) and the other

with a calcium-rich mineral surface (hydroxyapatite; Supporting Information Figure S4, Tables S2 and S3). In agreement with our hypothesis, electrostatic repulsion prevents association between the protein and the surface in the former case, while the presence of calcium in hydroxyapatite attenuates the repulsion between the negatively charged protein and the anionic phosphates, thus enabling protein–surface interaction.

A key aspect of the association thermodynamics between two molecules is the process of desolvation as the molecules approach each other. Studies in the past have reported that water molecules modulate the adsorption of biomolecules onto surfaces.[48,90−92] Indeed, experimental[93] and theoretical[94]
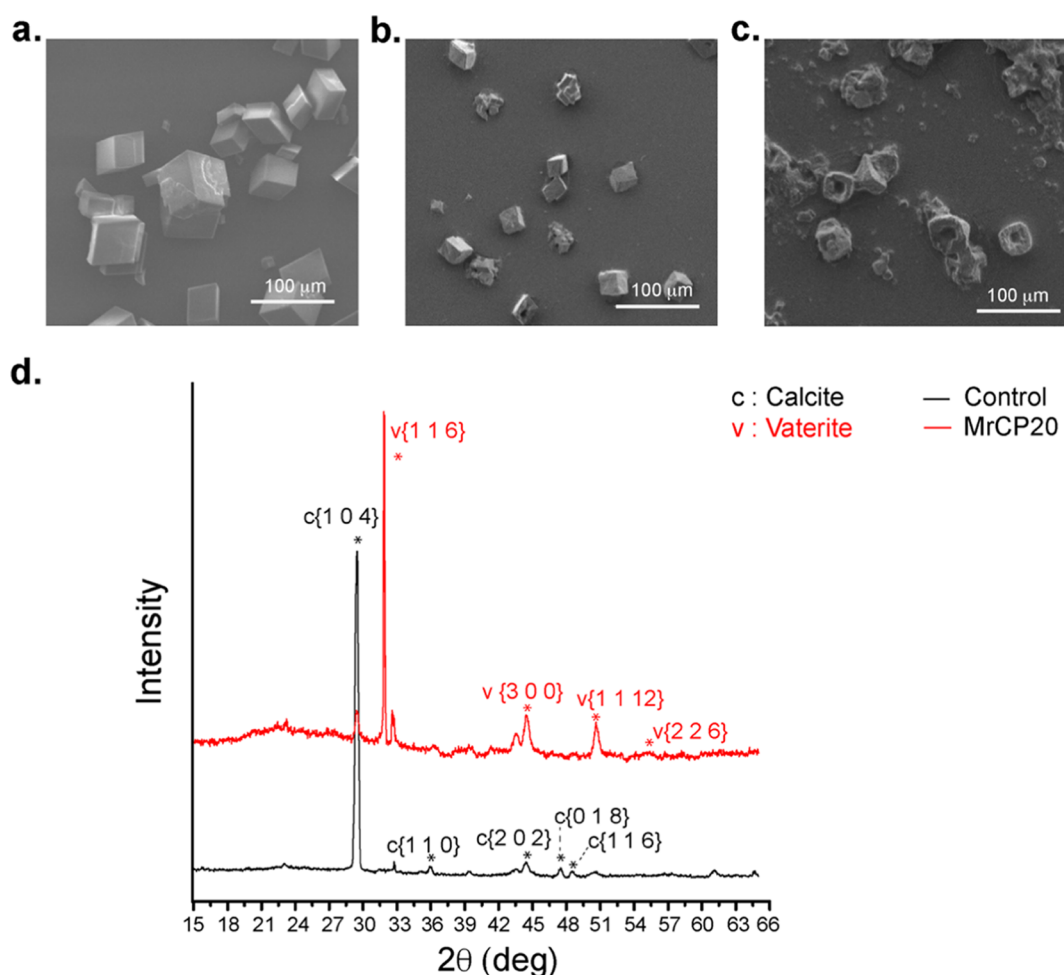
Figure 9. Characterization of calcium carbonate microcrystals. SEM micrographs (a) in the absence and (b, c) in the presence of 0.001 mg/mL MrCP20 (b) and 0.005 mg/mL MrCP20 (c). (d) XRD patterns of crystals in the presence (red line) and absence (control, black line) of MrCP20. The vaterite (v) and calcite (c) peaks are marked with reference to AMCSD[76] codes 0004854 and 0000098, respectively.

calculations have suggested that the calcite surface induces a substantial degree of water ordering at the interfaces, forming a layer of water molecules. In our simulations, it is clear that proximity to the calcite surface begins to affect the solvation shells that surround the protein as well as the calcite surface, and both surfaces experience dehydration (Figure 8).

Displacement of ordered water close to either the calcite surface or the protein surface is energetically (enthalpically) more expensive than displacing flexible water.[48] Therefore, the enthalpic energy gain as a result of protein binding will compensate for some of the energy loss due to the release of surface (calcite/protein)-bound water molecules. However, this release of bound water will result in a large increase in entropy and hence will thermodynamically stabilize the bound state of the protein. We saw earlier that the protein residues and ions can also be stabilized by bridging waters (for example, between the ions and acidic residues; Figure 5a−c). Hence, we expect the interaction between the protein and the surface also to be stabilized in a similar manner, as also observed previously in our study exploring green mussel adhesive proteins.[95]

Water molecules (up to 10 molecules; Table 3) bridge the acidic functional groups on the protein, stabilizing them into favorable water-mediated interactions with the oxygen atoms of CO_3^{2-} on the surface. This additional flexibility potentially allows multiple conformations of the protein to form stable

interactions with the surface (both direct and water-mediated), thus stabilizing the complex entropically. This flexibility will result in diverse conformations of the protein adsorbed on the surface, and each conformation will have characteristic interactions (direct and water-mediated) with the surface, including the release of some water molecules. For example, the number of water molecules present in the first water layer (up to 0.3 nm) of the calcite surface can be seen to vary as the protein is adsorbed (Table 3). Configuration 3 makes the strongest interaction with the surface; it has the highest number of residues interacting both directly through functional groups and indirectly through water, with the surface and also results in the largest release of water molecules (Tables 2 and 3). The penalty associated with desolvation as the ordered waters are released and as a freely diffusing protein is immobilized is compensated for by the interactions of the protein, as well as from the entropic gains associated with the release of ordered waters into the bulk phase. An estimate of $3RT$ has been associated with the entropic stabilization due to the release of each ordered water,[48] and this translates into gains of −75, −83, −162, and −128 kJ/(mol K) at 300 K for the four configurations in Table 3, respectively. Hence, it is clear that together with electrostatic stabilization, the interaction between the protein and the surface is also entropically stabilized to a large extent by the release of

ordered waters. Indeed, the observation that this protein can form amyloid fibrils on calcite surfaces may partly be driven by the entropic stabilization associated with dehydration.

We were also curious about the role of the Cys residues as they are abundant in MrCP20 (17%). NMR experiments suggest that 11% of the Cys residues are not engaged in any disulfide bonds,[41] and their role remains unclear. The relatively high abundance of free Cys may have evolved as a means of modulating the motion and stability of the interacting regions by either (i) engaging in intermolecular disulfide bonds with other molecules of MrCP20 or other cement proteins and/or (ii) interacting with the mineral via thiol bonds (S−Ca bond[79]). With a side-chain pKa of 8.0 (close to the pH range of seawater of 7.5−8.4), the thiol group on Cys can be easily deprotonated,[96] leading to a negatively charged sulfhydryl group, thereby boosting the acidic nature of the protein. In our simulations, we attempted to deprotonate the free Cys residues and explore the effect on calcite binding, but this led to an increased disorder in the protein as the net negative charge increased by 50%. Therefore, we could not arrive at a rigorous conclusion and hence did not proceed further; future work could explore this using multiscale simulations, which are beyond the scope of the current study.

Protein-Mediated Precipitation of Calcium Carbonate. To experimentally probe the above hypotheses on the ability of MrCP20 to regulate the assembly of $CaCO_3$, we used an established $CaCO_3$ mineralization method.[19] This consists of diffusing ammonium carbonate vapor through calcium chloride solution in the presence and absence (control) of a protein, which in our case is MrCP20, and monitoring the formation of $CaCO_3$ crystals.

In the absence of MrCP20, SEM micrographs indicated smooth $CaCO_3$ cubic crystals that appeared within 12 h (Figure 9a), and XRD patterns revealed that these crystals were made of calcite, as evidenced by the presence of {104}, {110}, and {202} reflections (Figure 9d). In the presence of MrCP20, micron-sized crystals of $CaCO_3$ were observed, which remained small even after 24 h (Figure 9b). At a low MrCP20 concentration, pseudospherical precipitated crystals were observed (Figure 9b), indicating coexisting morphologies. However, at a higher MrCP20 concentration, the crystals featured a distinct spherulite-like morphology (Figure 9c), which were identified as the less stable vaterite polymorph of $CaCO_3$ by XRD, as evidenced by the presence of {116} and {300} vaterite reflections (Figure 9d). $CaCO_3$ polymorphs identified in mature barnacles shells are calcite and aragonite[12,97,98] with no evidence of vaterite. In a systematic study, it was clearly depicted that calcite crystallization is a two-stage pathway proceeding from amorphous calcium carbonate to calcite via vaterite as a transient phase.[99] Additionally, previous studies have also revealed that organic additives can selectively allow the development of specific crystal faces, while inhibiting others.[100−102] Vaterite crystals typically exhibit a spherulite morphology,[99] which would be consistent with a radial crystal growth expected from the radial arrangement of ions around the protein surface observed in the free-ion simulations above (Figure 2b−d). Thus, MrCP20 appears to kinetically stabilize the less stable vaterite polymorph as a transient phase in the mineralization pathway toward the final mature shell made of calcite. A follow-up experimental study complementing these findings with additional electron diffraction, solid-state NMR spectroscopy, and infrared spectroscopy data will be presented in a separate publication.

The physical basis of the interactions between the crystals and MrCP20 is likely to be electrostatic since the zeta potential of freshly prepared pure $CaCO_3$ crystals is known to be positive,[103] whereas the net surface charge of the MrCP20 is negative at the pH of seawater (∼8).[14] Indeed, this is what we observed in the MD simulations, with acidic residues of MrCP20 predominantly driving $CaCO_3$ assembly and interactions with the calcite surface. Picker et al.[85] have suggested that Glu and Asp amino acids impact the solubility of amorphous $CaCO_3$ (intermediate precursor to the formation of the more thermodynamically stable polymorphs like calcite), implying that these residues either interact with the surface or modify the structure of $CaCO_3$ during precipitation. The interactions of the protein with the ions or the specific surface planes of calcite could influence the morphology of the crystal lattice. It is likely that such strong molecular interactions disrupt or delay the formation of a typical calcite crystal, initially leading to the formation of the less stable vaterite polymorph as observed (Figure 9b−d), and the steric barrier might eventually inhibit crystal growth. Consequently, it is observed that the size of the microcrystals formed in the presence of MrCP20 is relatively small.

Together, these observations in corroboration with previous experimental reports[14,19,42] suggest that MrCP20 exhibits significant affinity for calcium carbonate and influences the morphology of crystalline $CaCO_3$, as observed in our MD simulations. These results also indicate that MrCP20 is a good candidate for the modification of calcium carbonate morphology.

CONCLUSIONS

Molecular dynamics simulations of the barnacle cement protein MrCP20 suggest that the high surface charge on the protein is functionally important for its interactions with $CaCO_3$. The large number of anionic residues in the protein results in intramolecular electrostatic repulsions, generating ensembles of interconverting highly flexible conformations. These, in turn, enable rapid sequestration of Ca^{2+} and CO_3^{2-} ions and fidelity in regulating mineralization. The clustering of Ca^{2+} and CO_3^{2-} ions around specific charged sites in the protein underscores their role in regulating the nucleation of ions into assemblies, and subsequently in the interaction of the protein with the calcite surface. Additionally, the charged residues also sequester the shorter polar side chains (such as Asn, Ser, and Thr) and/or Tyr/His residues and water molecules to further enhance the interactions with the calcite surface. The final configuration of MrCP20 with calcite illustrates that: (i) the distribution of charged functional groups across the protein surface potentially provides it with abundant opportunities to facilitate binding in multiple orientations with the surface; (ii) there is no singular motif that mediates the protein−calcite interactions; and (iii) the charged residues and atoms with hydrogen bonding potential are used in an integrated manner, including mediation by water molecules, for surface interactions. Alternatively, this also supports the hypothesis that the protein is capable of interacting with other biomolecules, similar surfaces, or ions. In conclusion, it appears that MrCP20 potentially plays multiple functional roles in the underwater attachment of barnacles, including the regulation of biomineralization by concentrating inorganic ions, inhibiting radial growth of

$CaCO_3$ at the cement interaction site, and mediating adhesion with the mineral substrate.

■ ASSOCIATED CONTENT

ⓈⒾ Supporting Information

The Supporting Information is available free of charge at https://pubs.acs.org/doi/10.1021/acs.chemmater.0c02319.

Calculation details for the number of ions to be incorporated in the free-ion simulation systems; methods for control surface (HA and silica) simulations; figures with the evolution of RMSD, RMSF, and secondary structural features of MrCP20 in the presence of free ions; a table listing protein residues that interact with ionic clusters; snapshots from the MD simulations of MrCP20 in the presence of {10$\overline{1}$4} calcite surface, in the initial and final states; secondary structural evolution of MrCP20 in the presence of calcite; and results for control surface simulations of MrCP20 with HA and silica surface (PDF)

■ AUTHOR INFORMATION

Corresponding Authors

Chandra S. Verma − *Bioinformatics Institute, A*STAR, Singapore 138671; School of Biological Sciences, NTU, Singapore 636921; Department of Biological Sciences, NUS, Singapore 117558;* ⓞ orcid.org/0000-0003-0733-9798; Email: chandra@bii.a-star.edu.sg

Ali Miserez − *Biological and Biomimetic Material Laboratory, Center for Biomimetic Sensor Science, School of Materials Science and Engineering, Nanyang Technological University (NTU), Singapore 637553; School of Biological Sciences, NTU, Singapore 636921;* ⓞ orcid.org/0000-0003-0864-8170; Email: ali.miserez@ntu.edu.sg

Authors

Akshita Kumar − *Biological and Biomimetic Material Laboratory, Center for Biomimetic Sensor Science, School of Materials Science and Engineering, Nanyang Technological University (NTU), Singapore 637553; Bioinformatics Institute, A*STAR, Singapore 138671*

Harini Mohanram − *Biological and Biomimetic Material Laboratory, Center for Biomimetic Sensor Science, School of Materials Science and Engineering, Nanyang Technological University (NTU), Singapore 637553*

Jianguo Li − *Bioinformatics Institute, A*STAR, Singapore 138671;* ⓞ orcid.org/0000-0002-5544-6451

Hortense Le Ferrand − *School of Mechanical and Aerospace Engineering and School of Materials Science and Engineering, NTU, Singapore 639798;* ⓞ orcid.org/0000-0003-3017-9403

Complete contact information is available at:
https://pubs.acs.org/10.1021/acs.chemmater.0c02319

Author Contributions

A.K. performed the simulations and analysis. J.L. assisted in calcite, silica, and hydroxyapatite surface preparation and parametrization for the simulations. H.M. performed the mineralization experiments. H.L.F. assisted in acquisition of SEM micrographs and XRD diffraction. A.K., C.S.V., and A.M. prepared the manuscript.

■ REFERENCES

(1) Crisp, D. J. The Behaviour of Barnacle Cyprids in Relation to Water Movement over a Surface. *J. Exp. Biol.* **1955**, *32*, 569−590.

(2) Crisp, D. J.; Meadows, P. S.; Brambell, F. W. R. Adsorbed layers: the stimulus to settlement in barnacles. *Proc. R. Soc. Lond. Ser. B* **1963**, *158*, 364−387.

(3) Barnes, H.; Blackstock, J. The biochemical composition of the cement of a pedunculate cirripede. *J. Exp. Mar. Biol. Ecol.* **1974**, *16*, 87−91.

(4) Aldred, N.; Clare, A. S. The adhesive strategies of cyprids and development of barnacle-resistant marine coatings. *Biofouling* **2008**, *24*, 351−363.

(5) Gohad, N. V.; Aldred, N.; Orihuela, B.; Clare, A. S.; Rittschof, D.; Mount, A. S. Observations on the settlement and cementation of barnacle (*Balanus amphitrite*) cyprid larvae after artificial exposure to noradrenaline and the locations of adrenergic-like receptors. *J. Exp. Mar. Biol. Ecol.* **2012**, *416-417*, 153−161.

(6) Maruzzo, D.; Aldred, N.; Clare, A. S.; Hoeg, J. T. Metamorphosis in the cirripede crustacean Balanus amphitrite. *PLoS One* **2012**, *7*, No. e37408.

(7) Crisp, D. J.; Walker, G.; Young, G. A.; Yule, A. B. Adhesion and substrate choice in mussels and barnacles. *J. Colloid Interface Sci.* **1985**, *104*, 40−50.

(8) Saroyan, J. R.; Lindner, E.; Dooley, C. A. Repair and Reattachment in the Balanidae as Related to Their Cementing Mechanism. *Biol. Bull.* **1970**, *139*, 333−350.

(9) Waite, J. H. Nature's underwater adhesive specialist. *Int. J. Adhes. Adhesives* **1987**, *7*, 9−14.

(10) Walker, G. The Biochemical Composition of the Cement of two Barnacle Species, Balanus Hameri and Balanus Crenatus. *J. Mar. Biol. Assoc. U.K.* **1972**, *52*, 429−435.

(11) Essock-Burns, T.; Gohad, N. V.; Orihuela, B.; Mount, A. S.; Spillmann, C. M.; Wahl, K. J.; Rittschof, D. Barnacle biology before, during and after settlement and metamorphosis: a study of the interface. *J. Exp. Biol.* **2017**, *220*, 194−207.

(12) Burden, D. K.; Spillmann, C. M.; Everett, R. K.; Barlow, D. E.; Orihuela, B.; Deschamps, J. R.; Fears, K. P.; Rittschof, D.; Wahl, K. J. Growth and development of the barnacle Amphibalanus amphitrite: time and spatially resolved structure and chemistry of the base plate. *Biofouling* **2014**, *30*, 799−812.

(13) Yule, A. B.; W, G. Adhesion in Barnacles, In *Barnacle Biology*, Southward, A. J., Eds.; A. A. Balkema: Rotterdam, 1987; pp 389−402.

(14) Mori, Y.; Urushida, Y.; Nakano, M.; Uchiyama, S.; Kamino, K. Calcite-specific coupling protein in barnacle underwater cement. *FEBS J.* **2007**, *274*, 6436−6446.

(15) Callow, M. E.; Callow, J. E. Marine biofouling: a sticky problem. *Biologist* **2002**, *49*, 10−14.

(16) Schultz, M. P.; Bendick, J. A.; Holm, E. R.; Hertel, W. M. Economic impact of biofouling on a naval surface ship. *Biofouling* **2011**, *27*, 87−98.

(17) Liang, C.; Ye, Z.; Xue, B.; Zeng, L.; Wu, W.; Zhong, C.; Cao, Y.; Hu, B.; Messersmith, P. B. Self-Assembled Nanofibers for Strong Underwater Adhesion: The Trick of Barnacles. *ACS Appl. Mater. Interfaces* **2018**, *10*, 25017−25025.

(18) Senkbeil, T.; Mohamed, T.; Simon, R.; Batchelor, D.; Di Fino, A.; Aldred, N.; Clare, A. S.; Rosenhahn, A. In vivo and in situ

synchrotron radiation-based mu-XRF reveals elemental distributions during the early attachment phase of barnacle larvae and juvenile barnacles. *Anal. Bioanal. Chem.* **2016**, *408*, 1487−1496.

(19) So, C. R.; Liu, J.; Fears, K. P.; Leary, D. H.; Golden, J. P.; Wahl, K. J. Self-Assembly of Protein Nanofibrils Orchestrates Calcite Step Movement through Selective Nonchiral Interactions. *ACS Nano* **2015**, *9*, 5782−5791.

(20) So, C. R.; Scancella, J. M.; Fears, K. P.; Essock-Burns, T.; Haynes, S. E.; Leary, D. H.; Diana, Z.; Wang, C.; North, S.; Oh, C. S.; Wang, Z.; Orihuela, B.; Rittschof, D.; Spillmann, C. M.; Wahl, K. J. Oxidase Activity of the Barnacle Adhesive Interface Involves Peroxide-Dependent Catechol Oxidase and Lysyl Oxidase Enzymes. *ACS Appl. Mater. Interfaces* **2017**, *9*, 11493−11505.

(21) So, C. R.; Fears, K. P.; Leary, D. H.; Scancella, J. M.; Wang, Z.; Liu, J. L.; Orihuela, B.; Rittschof, D.; Spillmann, C. M.; Wahl, K. J. Sequence basis of Barnacle Cement Nanostructure is Defined by Proteins with Silk Homology. *Sci. Rep.* **2016**, *6*, No. 36219.

(22) Rocha, M.; Antas, P.; Castro, L. F. C.; Campos, A.; Vasconcelos, V.; Pereira, F.; Cunha, I. Comparative Analysis of the Adhesive Proteins of the Adult Stalked Goose Barnacle *Pollicipes pollicipes* (Cirripedia: Pedunculata). *Mar. Biotechnol.* **2019**, *21*, 38−51.

(23) Raman, S.; Malms, L.; Utzig, T.; Shrestha, B. R.; Stock, P.; Krishnan, S.; Valtiner, M. Adhesive barnacle peptides exhibit a steric-driven design rule to enhance adhesion between asymmetric surfaces. *Colloids Surf., B* **2017**, *152*, 42−48.

(24) So, C. R.; Yates, E.; Estrella, L.; Schenck, A.; Yip, C.; Wahl, K. J. Wet Adhesive Nanomaterials Inspired by the Barnacle Adhesive. *Biophys. J.* **2018**, *114*, 192a−193a.

(25) So, C. R.; Yates, E. A.; Estrella, L. A.; Fears, K. P.; Schenck, A. M.; Yip, C. M.; Wahl, K. J. Molecular Recognition of Structures Is Key in the Polymerization of Patterned Barnacle Adhesive Sequences. *ACS Nano* **2019**, *13*, 5172−5183.

(26) Kamino, K.; Inoue, K.; Maruyama, T.; Takamatsu, N.; Harayama, S.; Shizuri, Y. Barnacle cement proteins. Importance of disulfide bonds in their insolubility. *J. Biol. Chem.* **2000**, *275*, 27360−27365.

(27) Fears, K. P.; Orihuela, B.; Rittschof, D.; Wahl, K. J. Acorn Barnacles Secrete Phase-Separating Fluid to Clear Surfaces Ahead of Cement Deposition. *Adv. Sci.* **2018**, *5*, No. 1700762.

(28) Barlow, D. E.; Dickinson, G. H.; Orihuela, B.; Rittschof, D.; Wahl, K. J. In situ ATR-FTIR characterization of primary cement interfaces of the barnacle Balanus amphitrite. *Biofouling* **2009**, *25*, 359−366.

(29) Barlow, D. E.; Dickinson, G. H.; Orihuela, B.; Kulp, J. L., 3rd; Rittschof, D.; Wahl, K. J. Characterization of the adhesive plaque of the barnacle Balanus amphitrite: amyloid-like nanofibrils are a major component. *Langmuir* **2010**, *26*, 6549−6556.

(30) Evans, J. S. Aragonite-associated biomineralization proteins are disordered and contain interactive motifs. *Bioinformatics* **2012**, *28*, 3182−3185.

(31) Pendola, M.; Jain, G.; Evans, J. S. Skeletal development in the sea urchin relies upon protein families that contain intrinsic disorder, aggregation-prone, and conserved globular interactive domains. *PLoS One* **2019**, *14*, No. e0222068.

(32) Kamino, K.; Odo, S.; Maruyama, T. Cement proteins of the acorn barnacle, *Megabalanus rosa. Biol. Bull.* **1996**, *190*, 403−409.

(33) Urushida, Y.; Nakano, M.; Matsuda, S.; Inoue, N.; Kanai, S.; Kitamura, N.; Nishino, T.; Kamino, K. Identification and functional characterization of a novel barnacle cement protein. *FEBS J.* **2007**, *274*, 4336−4346.

(34) Sullan, R. M.; Gunari, N.; Tanur, A. E.; Chan, Y.; Dickinson, G. H.; Orihuela, B.; Rittschof, D.; Walker, G. C. Nanoscale structures and mechanics of barnacle cement. *Biofouling* **2009**, *25*, 263−275.

(35) Kamino, K.; Nakano, M.; Kanai, S. Significance of the conformation of building blocks in curing of barnacle underwater adhesive. *FEBS J.* **2012**, *279*, 1750−1760.

(36) Nakano, M.; Kamino, K. Amyloid-like conformation and interaction for the self-assembly in barnacle underwater cement. *Biochemistry* **2015**, *54*, 826−835.

(37) Kamino, K. Barnacle Underwater Attachment, In *Biological Adhesives*, Smith, A. M., Eds.; Springer: Berlin, Heidelberg, 2006; pp 145−166.

(38) Kamino, K. Novel barnacle underwater adhesive protein is a charged amino acid-rich protein constituted by a Cys-rich repetitive sequence. *Biochem. J.* **2001**, *356*, 503−507.

(39) Suzuki, R.; Mori, Y.; Kamino, K.; Yamazaki, T. NMR assignment of the barnacle cement protein mrcp-20k. *J. Biomol. NMR* **2005**, *32*, 257.

(40) Wiegemann, M.; Watermann, B. Peculiarities of barnacle adhesive cured on non-stick surfaces. *J. Adhes. Sci. Technol.* **2003**, *17*, 1957−1977.

(41) Mohanram, H.; Kumar, A.; Verma, C. S.; Pervushin, K.; Miserez, A. Three-dimensional structure of Megabalanus rosa Cement Protein 20 revealed by multi-dimensional NMR and molecular dynamics simulations. *Philos. Trans. R. Soc. Lond. Ser. B* **2019**, *374*, No. 20190198.

(42) Liang, C.; Strickland, J.; Ye, Z.; Wu, W.; Hu, B.; Rittschof, D. Biochemistry of Barnacle Adhesion: An Updated Review. *Front. Mar. Sci.* **2019**, *6*, No. 565.

(43) He, L. S.; Zhang, G.; Qian, P. Y. Characterization of two 20kDa-cement protein (cp20k) homologues in Amphibalanus amphitrite. *PLoS One* **2013**, *8*, No. e64130.

(44) Lin, H. C.; Wong, Y. H.; Tsang, L. M.; Chu, K. H.; Qian, P. Y.; Chan, B. K. First study on gene expression of cement proteins and potential adhesion-related genes of a membranous-based barnacle as revealed from Next-Generation Sequencing technology. *Biofouling* **2014**, *30*, 169−181.

(45) Boskey, A. L.; Villarreal-Ramirez, E. Intrinsically disordered proteins and biomineralization. *Matrix Biol.* **2016**, *52-54*, 43−59.

(46) Elsharkawy, S.; Al-Jawad, M.; Pantano, M. F.; Tejeda-Montes, E.; Mehta, K.; Jamal, H.; Agarwal, S.; Shuturminska, K.; Rice, A.; Tarakina, N. V.; Wilson, R. M.; Bushby, A. J.; Alonso, M.; Rodriguez-Cabello, J. C.; Barbieri, E.; Del Rio Hernandez, A.; Stevens, M. M.; Pugno, N. M.; Anderson, P.; Mata, A. Protein disorder-order interplay to guide the growth of hierarchical mineralized structures. *Nat. Commun.* **2018**, *9*, No. 2145.

(47) Rao, A.; Drechsler, M.; Schiller, S.; Scheffner, M.; Gebauer, D.; Cölfen, H. Stabilization of Mineral Precursors by Intrinsically Disordered Proteins. *Adv. Funct. Mater.* **2018**, *28*, No. 1802063.

(48) Freeman, C. L.; Harding, J. H.; Quigley, D.; Rodger, P. M. Simulations of Ovocleidin-17 Binding to Calcite Surfaces and Its Implications for Eggshell Formation. *J. Phys. Chem. C* **2011**, *115*, 8175−8183.

(49) Xue, Z.; Shen, Q.; Liang, L.; Shen, J.-W.; Wang, Q. Adsorption Behavior and Mechanism of SCA-1 on a Calcite Surface: A Molecular Dynamics Study. *Langmuir* **2017**, *33*, 11321−11331.

(50) Innocenti Malini, R.; Finney, A. R.; Hall, S. A.; Freeman, C. L.; Harding, J. H. The Water−Amorphous Calcium Carbonate Interface and Its Interactions with Amino Acids. *Cryst. Growth Des.* **2017**, *17*, 5811−5822.

(51) Rani, R. S.; Saharay, M. Molecular dynamics simulation of protein-mediated biomineralization of amorphous calcium carbonate. *RSC Adv.* **2019**, *9*, 1653−1663.

(52) Zhao, W.; Wang, Z.; Xu, Z.; Sahai, N. Osteocalcin facilitates calcium phosphate ion complex growth as revealed by free energy calculation. *Phys. Chem. Chem. Phys.* **2018**, *20*, 13047−13056.

(53) Dolinsky, T. J.; Nielsen, J. E.; McCammon, J. A.; Baker, N. A. PDB2PQR: an automated pipeline for the setup of Poisson-Boltzmann electrostatics calculations. *Nucleic Acids Res.* **2004**, *32*, W665−7.

(54) Martínez, L.; Andrade, R.; Birgin, E. G.; Martinez, J. M. PACKMOL: a package for building initial configurations for molecular dynamics simulations. *J. Comput. Chem.* **2009**, *30*, 2157−2164.

(55) Jorgensen, W. L.; Chandrasekhar, J.; Madura, J. D.; Impey, R. W.; Klein, M. L. Comparison of simple potential functions for simulating liquid water. *J. Chem. Phys.* **1983**, *79*, 926−935.

(56) Wang, J.; Wang, W.; Kollman, P. A.; Case, D. A. Automatic atom type and bond type perception in molecular mechanical calculations. *J. Mol. Graphics Model.* **2006**, *25*, 247−260.

(57) Cornell, W. D.; Cieplak, P.; Bayly, C. I.; Gould, I. R.; Merz, K. M.; Ferguson, D. M.; Spellmeyer, D. C.; Fox, T.; Caldwell, J. W.; Kollman, P. A. A second generation force field for the simulation of proteins, nucleic acids, and organic molecules. *J. Am. Chem. Soc.* **1995**, *117*, 5179−5197.

(58) Wang, J.; Wolf, R. M.; Caldwell, J. W.; Kollman, P. A.; Case, D. A. Development and testing of a general amber force field. *J. Comput. Chem.* **2004**, *25*, 1157−1174.

(59) Case, D. A.; B, V.; Berryman, J. T.; Betz, R. M.; Cai, Q.; Cerutti, D. S.; Cheatham, T. E., III; Darden, T. A.; Duke, R. E.; Gohlke, H.; Goetz, A. W.; Gusarov, S.; Homeyer, N.; Janowski, P.; Kaus, J.; Kolossváry, I.; Kovalenko, A.; Lee, T. S.; LeGrand, S.; Luchko, T.; Luo, R.; Madej, B.; Merz, K. M.; Paesani, F.; Roe, D. R.; Roitberg, A.; Sagui, C.; Salomon-Ferrer, R.; Seabra, G.; Simmerling, C. L.; Smith, W.; Swails, J.; Walker, R. C.; Wang, J.; Wolf, R. M.; Wu, X.; Kollman, P. A.. *AMBER 14*; University of California: San Francisco, 2014.

(60) Ryckaert, J.-P.; Ciccotti, G.; Berendsen, H. J. C. Numerical integration of the cartesian equations of motion of a system with constraints: molecular dynamics of n-alkanes. *J. Comput. Phys.* **1977**, *23*, 327−341.

(61) Darden, T.; York, D.; Pedersen, L. Particle mesh Ewald: An N· log(N) method for Ewald sums in large systems. *J. Chem. Phys.* **1993**, *98*, 10089−10092.

(62) Berendsen, H. J. C.; Postma, J. P. M.; Gunsteren, W. F. v.; DiNola, A.; Haak, J. R. Molecular dynamics with coupling to an external bath. *J. Chem. Phys.* **1984**, *81*, 3684−3690.

(63) Humphrey, W.; Dalke, A.; Schulten, K. VMD: visual molecular dynamics. *J. Mol. Graphics* **1996**, *14*, 33−38.

(64) *The PyMOL Molecular Graphics System*, version 2.4.0; Schrödinger, LLC.

(65) Pettersen, E. F.; Goddard, T. D.; Huang, C. C.; Couch, G. S.; Greenblatt, D. M.; Meng, E. C.; Ferrin, T. E. UCSF Chimera–a visualization system for exploratory research and analysis. *J. Comput. Chem.* **2004**, *25*, 1605−1612.

(66) XMGRACE. *Center for Coastal and Land-Margin Research*, version 1.5.1; Oregon Graduate Institute of Science and Technology: Beaverton, OR, 2005.

(67) Dassault Systèmes. *Materials Studio*; Dassault Systèmes BIOVIA: San Diego, 2018.

(68) Abraham, M. J.; Murtola, T.; Schulz, R.; Páll, S.; Smith, J. C.; Hess, B.; Lindahl, E. GROMACS: High performance molecular simulations through multi-level parallelism from laptops to super-computers. *SoftwareX* **2015**, *1-2*, 19−25.

(69) Xiao, S.; Edwards, S. A.; Gräter, F. A New Transferable Forcefield for Simulating the Mechanics of CaCO3 Crystals. *J. Phys. Chem. C* **2011**, *115*, 20067−20075.

(70) Ukrainczyk, M.; Greiner, M.; Elts, E.; Briesen, H. Simulating preferential sorption of tartrate on prismatic calcite surfaces. *CrystEngComm* **2015**, *17*, 149−159.

(71) Evans, D. J.; Holian, B. L. The Nose−Hoover thermostat. *J. Chem. Phys.* **1985**, *83*, 4069−4074.

(72) Parrinello, M.; Rahman, A. Polymorphic transitions in single crystals: A new molecular dynamics method. *J. Appl. Phys.* **1981**, *52*, 7182−7190.

(73) Parrinello, M.; Rahman, A. Crystal Structure and Pair Potentials: A Molecular-Dynamics Study. *Phys. Rev. Lett.* **1980**, *45*, 1196−1199.

(74) Mann, K.; Siedler, F.; Treccani, L.; Heinemann, F.; Fritz, M. Perlinhibin, a cysteine-, histidine-, and arginine-rich miniprotein from abalone (Haliotis laevigata) nacre, inhibits in vitro calcium carbonate crystallization. *Biophys. J.* **2007**, *93*, 1246−1254.

(75) Zhao, K.; Wang, M.; Wang, X.; Wu, C.; Xu, H.; Lu, J. R. Crystal Growth of Calcite Mediated by Ovalbumin and Lysozyme: Atomic Force Microscopy Study. *Cryst. Growth Des.* **2013**, *13*, 1583−1589.

(76) Downs, R. T.; Hall-Wallace, M. The American Mineralogist crystal structure database. *Am. Mineral.* **2003**, *88*, 247−250.

(77) Boskey, A. L. Biomineralization: an overview. *Connect. Tissue Res.* **2003**, *44*, 5−9.

(78) Michenfelder, M.; Fu, G.; Lawrence, C.; Weaver, J. C.; Wustman, B. A.; Taranto, L.; Evans, J. S.; Morse, D. E. Character-ization of two molluscan crystal-modulating biomineralization proteins and identification of putative mineral binding domains. *Biopolymers* **2003**, *70*, 522−533.

(79) Borukhin, S.; Bloch, L.; Radlauer, T.; Hill, A. H.; Fitch, A. N.; Pokroy, B. Screening the Incorporation of Amino Acids into an Inorganic Crystalline Host: the Case of Calcite. *Adv. Funct. Mater.* **2012**, *22*, 4216−4224.

(80) Azzopardi, P. V.; O'Young, J.; Lajoie, G.; Karttunen, M.; Goldberg, H. A.; Hunter, G. K. Roles of electrostatics and conformation in protein-crystal interactions. *PLoS One* **2010**, *5*, No. e9330.

(81) Tavafoghi, M.; Cerruti, M. The role of amino acids in hydroxyapatite mineralization. *J. R. Soc. Interface* **2016**, *13*, No. 20160462.

(82) Weiner, S.; Hood, L. Soluble protein of the organic matrix of mollusk shells: a potential template for shell formation. *Science* **1975**, *190*, 987−989.

(83) Marin, F.; Roy, Le.; Marie, N. B., The formation and mineralization of mollusk shell. *Front. Biosci.* **2012**, *4*, 1099−1125.

(84) Evans, J. S. "Tuning in" to mollusk shell nacre- and prismatic-associated protein terminal sequences. Implications for biomineraliza-tion and the construction of high performance inorganic-organic composites. *Chem. Rev.* **2008**, *108*, 4455−4462.

(85) Picker, A.; Kellermeier, M.; Seto, J.; Gebauer, D.; Cölfen, H. The multiple effects of amino acids on the early stages of calcium carbonate crystallization. *Z. Kristallogr.* **2012**, *227*, 744.

(86) Finney, A. R.; Innocenti Malini, R.; Freeman, C. L.; Harding, J. H. Amino Acid and Oligopeptide Effects on Calcium Carbonate Solutions. *Cryst. Growth Des.* **2020**, *20*, 3077−3092.

(87) Collino, S.; Evans, J. S. Structural features that distinguish kinetically distinct biomineralization polypeptides. *Biomacromolecules* **2007**, *8*, 1686−1694.

(88) Collino, S.; Evans, J. S. Molecular specifications of a mineral modulation sequence derived from the aragonite-promoting protein n16. *Biomacromolecules* **2008**, *9*, 1909−1918.

(89) Kim, I. W.; Darragh, M. R.; Orme, C.; Evans, J. S. Molecular "Tuning" of Crystal Growth by Nacre-Associated Polypeptides. *Cryst. Growth Des.* **2006**, *6*, 5−10.

(90) Kerisit, S.; Parker, S. C. Free Energy of Adsorption of Water and Metal Ions on the {10$\bar{1}$4} Calcite Surface. *J. Am. Chem. Soc.* **2004**, *126*, 10152−10161.

(91) Elhadj, S.; Salter, E. A.; Wierzbicki, A.; De Yoreo, J. J.; Han, N.; Dove, P. M. Peptide Controls on Calcite Mineralization: Poly-aspartate Chain Length Affects Growth Kinetics and Acts as a Stereochemical Switch on Morphology. *Cryst. Growth Des.* **2006**, *6*, 197−201.

(92) Freeman, C. L.; Asteriadis, I.; Yang, M.; Harding, J. H. Interactions of Organic Molecules with Calcite and Magnesite Surfaces. *J. Phys. Chem. C* **2009**, *113*, 3666−3673.

(93) Fenter, P.; Geissbühler, P.; DiMasi, E.; Srajer, G.; Sorensen, L. B.; Sturchio, N. C. Surface speciation of calcite observed in situ by high-resolution X-ray reflectivity. *Geochim. Cosmochim. Acta* **2000**, *64*, 1221−1228.

(94) Kerisit, S.; Cooke, D. J.; Spagnoli, D.; Parker, S. C. Molecular dynamics simulations of the interactions between water and inorganic solids. *J. Mater. Chem.* **2005**, *15*, 1454−1462.

(95) Petrone, L.; Kumar, A.; Sutanto, C. N.; Patil, N. J.; Kannan, S.; Palaniappan, A.; Amini, S.; Zappone, B.; Verma, C.; Miserez, A. Mussel adhesion is dictated by time-regulated secretion and molecular

conformation of mussel adhesive proteins. *Nat. Commun.* **2015**, *6*, No. 8737.

(96) Poole, L. B. The basics of thiols and cysteines in redox biology and chemistry. *Free Radical Biol. Med.* **2015**, *80*, 148−157.

(97) Bourget, E. Barnacle shells: composition, structure and growth. *Barnacle Biol.* **1987**, *5*, 267−285.

(98) Ullmann, C. V.; Gale, A. S.; Huggett, J.; Wray, D.; Frei, R.; Korte, C.; Broom-Fendley, S.; Littler, K.; Hesselbo, S. P. The geochemistry of modern calcareous barnacle shells and applications for palaeoenvironmental studies. *Geochim. Cosmochim. Acta* **2018**, *243*, 149−168.

(99) Rodriguez-Blanco, J. D.; Shaw, S.; Benning, L. G. The kinetics and mechanisms of amorphous calcium carbonate (ACC) crystallization to calcite, viavaterite. *Nanoscale* **2011**, *3*, 265−271.

(100) Sommerdijk, N. A. J. M.; With, Gd. Biomimetic CaCO3 Mineralization using Designer Molecules and Interfaces. *Chem. Rev.* **2008**, *108*, 4499−4550.

(101) Gower, L. B. Biomimetic Model Systems for Investigating the Amorphous Precursor Pathway and Its Role in Biomineralization. *Chem. Rev.* **2008**, *108*, 4551−4627.

(102) Meldrum, F. C.; Cölfen, H. Controlling Mineral Morphologies and Structures in Biological and Synthetic Systems. *Chem. Rev.* **2008**, *108*, 4332−4432.

(103) Chibowski, E.; Hotysz, L.; Szcześ, A. Time dependent changes in zeta potential of freshly precipitated calcium carbonate. *Colloids Surf., A* **2003**, *222*, 41−54.